A Comparative Study of Three Methodologies for Modeling Dynamic Stall

by
L. Sankar (Georgia Institute of Technology),
J. Zibi-Bailly, J.C. Le Balleur, D. Blaise, O. Rouzaud (ONERA Châtillon),
M. Rhee, C. Tung (U.S. Army Aeroflightdynamics Directorate (AFDD))

During the past two decades, there has been an increased reliance on the use of computational fluid dynamics methods for modeling rotors in high speed forward flight. Computational methods are being developed for modeling the shock induced loads on the advancing side, first-principles based modeling of the trailing wake evolution, and for retreating blade stall. The retreating blade dynamic stall problem has received particular attention, because the large variations in lift and pitching moments encountered in dynamic stall can lead to blade vibrations and pitch link fatigue.

Restricting to aerodynamics, the numerical prediction of dynamic stall is still a complex and challenging CFD problem, that, even in two dimensions at low speed, gathers the major difficulties of aerodynamics, such as the grid resolution requirements for the viscous phenomena at leading-edge bubbles or in mixing-layers, the bias of the numerical viscosity, and the major difficulties of the physical modeling, such as the turbulence models, the transition models, whose both determinant influences, already present in static maximal-lift or stall computations, are emphasized by the dynamic aspect of the phenomena.

In the framework of the US-France Memorandum of Agreement on Helicopter Aeromechanics, it has been decided first to compare the experimental 2D database performed by Piziali at US Army AFDD for an oscillating NACA0015 airfoil/wing with the results of three CFD codes :

- The DSS2 code, a Reynolds-Averaged Navier-Stokes (RANS) solver developed at Georgia Tech Institute (GIT), using a Beam-Warming scheme and an implicit time marching algorithm;
- The CANARI code, a Reynolds-Averaged Navier-Stokes solver developed at ONERA, that uses Jameson's scheme and a time implicit integration based on the dual time step method;
- The VIS05 code, a generalized Viscous-Inviscid Interaction (VII) solver developed at ONERA whose formulation access to deep stall, that uses time implicit schemes and strongly converges the viscous coupling each time step.

For both Navier-Stokes (NS) codes, the one transport equation Spalart-Allmaras model is used, and the flow is supposed, in the sense of this model, to be computed fully turbulent. For the VIS05 code, a two-equation 'k-u'v'-forced' turbulence model is used, and computations are at present performed with laminar-turbulent transition prescribed at 0.5% chord on the upper side of the airfoil. The present computations are performed on a common C-H type medium grid of 257x129 points for the NS codes, and on a grid 257x(64+49) for the VII code with 49 adaptive nodes normal to the viscous layer and identical wall nodes as in the NS codes.

In order to better estimate the CFD state-of-the-art of the codes in the dynamic regime, the static stall problem has been firstly studied. The lift slope predictions in the quasi-linear part until $\alpha=12°$ are in good agreement with experiment for the three codes (Fig. 1a), the lift slope of the NS-GIT code being slightly smaller than the slope of the NS and VII ONERA codes.

Some discrepancies appear, with respect to experiment, for the prediction of the CLmax coefficient, somewhat under-estimated by the NS-GIT code as the lift-slope, and somewhat over-estimated by the NS-ONERA and VII-ONERA codes, the stall incidence occurring earlier for the NS-GIT code, and later for both NS and VII ONERA codes. Consequently also, the pitching moment coefficient evolution (Fig. 1b) of the NS-GIT code appears slightly nearer experiment for the CMmax value and the incidence of the moment stall, the moment stall evolution being also reproduced by the VII ONERA code but at a slightly higher incidence, and being slightly delayed by the NS ONERA code. Around the stall incidence (α=14°), the streamlines show the generation of a trailing-edge re-circulation bubble. In the present context of fully turbulent and medium grid (257x129) RANS simulations, and of a 5% prescribed transition (upstream laminar separation) in the VII simulation, the extent of the separation is larger in the NS-GIT than in the NS and VII ONERA codes, which explains its earlier lift and moment stalls.

For unsteady configurations, a moderate stall case is analyzed for two reduced frequencies $k=\omega c/2V_\infty$, equal to 0.095 and 0.038 (incidence law $\alpha(t)=11°+4°\sin(\omega t)$, $M_\infty=0.289$, $Re=1.949\times10^6$). The well-known unsteady effects of dynamic stall are observed in experiment (Fig. 3a), with an increase of the maximum lift, and a delay of stall with respect to the steady case. The NS-GIT and VII-ONERA computations predict quite correctly these effects (Fig. 3b-3d), contrary to the NS-ONERA code (Fig. 3c). Furthermore, it can be seen from the experimental data that the decrease of the reduced frequency provides a more pronounced stall. This trend is well predicted by the VII-ONERA code, with more difficulty by the two Navier-Stokes codes.

The comparisons with experiment of the computed aerodynamic coefficients for the test case $\alpha(t)=11°+4°\sin(\omega t)$, k=0.038, are shown in Figures 4a-4b. Some discrepancies exist between the results of the three computations. Both NS and VII ONERA calculations are in good agreement with experiment in the linear part of the lift hysteresis loop, while the NS-GIT result under-estimates the lift coefficient. All the three codes cannot correctly predict the abrupt decrease of the pitching moment coefficient, as clearly seen in the experimental data.

These results illustrate at the present time the advances and weaknesses of numerical codes when predicting the difficult dynamic stall phenomenon. In the full paper, the complete sets of computational studies are provided including the detailed analysis of the pressure data for a better understanding of the unsteady flow characteristics occurring during dynamic motion of the airfoil. Additionally, the sensitive effects of grid density, numerical viscosity, transition models and locations, will be analyzed in detail, to allow a better understanding of both the behavior of the three methodologies, and of their expected further developments.

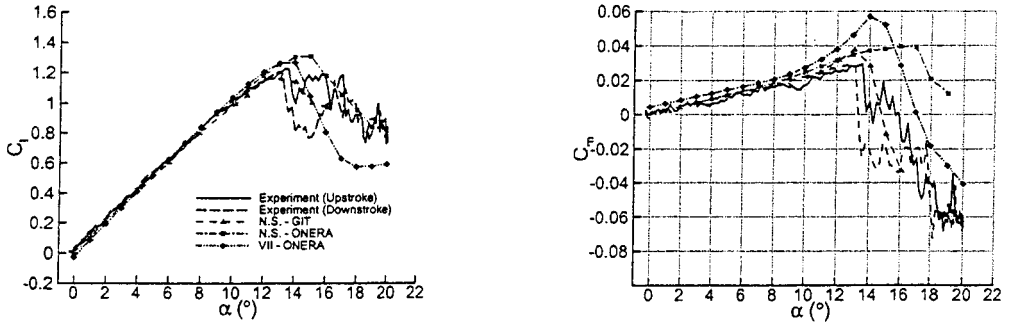

Figures 1a-1b : Static polars of lift and pitching moment coefficients

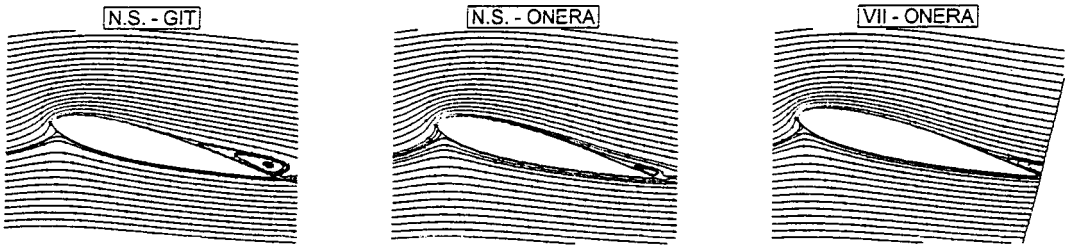

Figures 2a-2b-2c : Streamlines of the steady flow-field for α=14 ° (in the present treatments of laminar-turbulent transition).

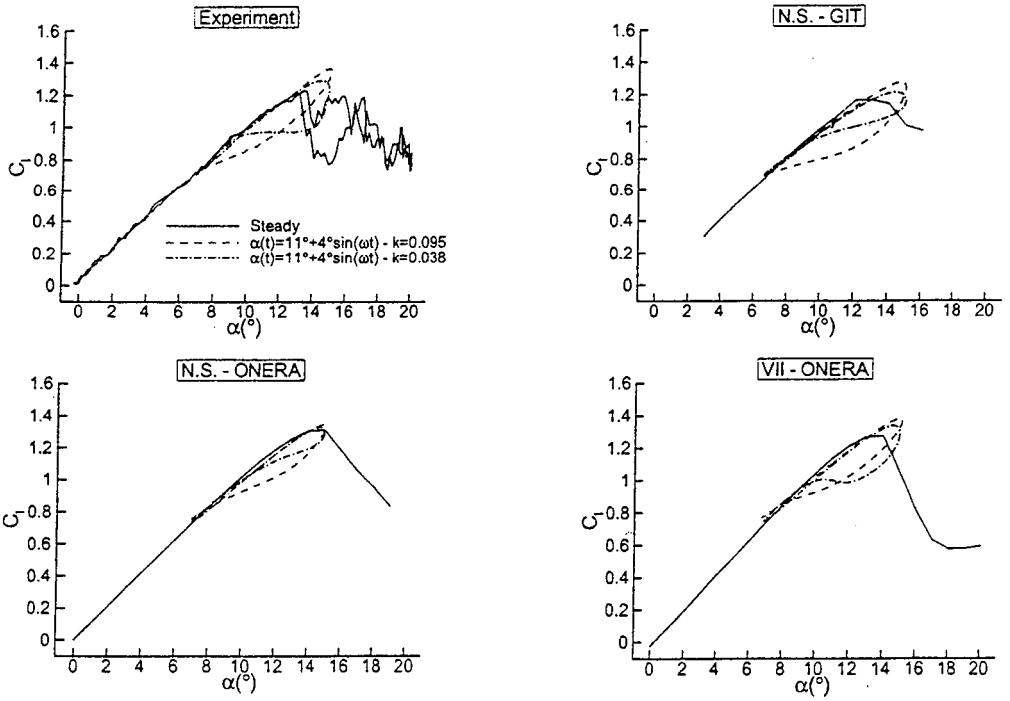

Figures 3a-3b-3c-3d : Influence of unsteady effects and reduced frequency effects on the lift coefficient

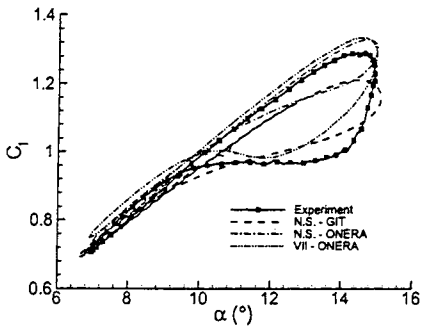

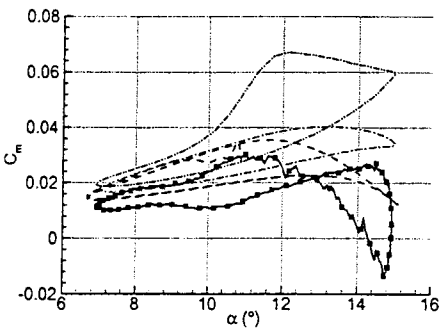

Figures 4a-4b : Comparisons of lift and pitching moment coefficients for $\alpha(t)=11°+4°\sin(\omega t)$, $k=0.038$